The critical role of N-vacancy on chemical composition fluctuations and degradation of InAlN layer

Ranim Mohamad, Marie Pierre Chauvat, Slawomir Kret, Piero Gamarra, Sylvain Delage, Viwanou Hounkpati, Cedric Lacam, Jun Chen, Pierre Ruterana

The critical role of N-vacancy on chemical composition fluctuations and degradation of InAlN layer

Ranim Mohamad[*,1], *Marie Pierre Chauvat*[1], *Slawomir Kret*[2], *Piero Gamarra*[3], *Sylvain Delage*[3], *Viwanou Hounkpati*[1], *Cedric Lacam*[3], *Jun Chen*[1], *and Pierre Ruterana*[1]

[1]Centre de Recherche sur les Ions, les Matériaux et la Photonique UMR 6252, CNRS ENSICAEN UCBN CEA, 6 Boulevard du Maréchal Juin, 14050 Caen Cedex, France.
[2]Institute of Physics, Polish Academy of Sciences, 32/46 al. Lotników, 02-668 Warsaw, Poland.
[3]III-V Lab, 1 Avenue Augustin Fresnel, Campus Polytechnique, 91767 Palaiseau, France.

Due to its intrinsic properties and the possible lattice match to GaN, InAlN is expected to allow the fabrication of optimal high electron mobility transistors for high power and high frequency applications. However, the crystal quality of InAlN nearly lattice-matched to GaN degrades when the layer thickness is increased, and this is a strong limitation for the fabrication of devices in which thick barriers need to be used. In this work, we have carried out a detailed theoretical investigation of the behavior of indium atoms in the alloy. It is clearly shown that in the presence of nitrogen vacancies, which are common defects in these materials, indium nitride clusters will present excess formation energy up to diameters around 1.4 nm. In parallel, Z contrast TEM observations close to the InAlN/GaN interface show that 2-5 nm size indium rich areas form and are systematically connected to the vertical degradation channels. This is at variance with published results, which concluded that the observed degradation was due exclusively either to the underlying threading dislocations or to a characteristic three-dimensional growth mode.

KEYWORDS: N-vacancy, InAlN degradation, atomistic modelling, In segregation, energetic stability, TEM, ab-initio.

I. INTRODUCTION

The outstanding properties of group III nitride (InN, AlN and GaN) compounds find application in light emitting diode (LEDs)[1], laser diode (LDs)[2] and high electron mobility transistors (HEMTs)[3]. In particular, the ternary InAlN alloy is a subject of much research effort due to its lattice match with GaN for a composition of indium around 18%, when grown along [0001]. Interestingly, the band gap of $In_xAl_{1-x}N$ alloys covers probably the widest wavelength range of known semiconductors (0.67 eV (InN)[4] to 6.2 eV (AlN)[5]), however this unique property comes along with many challenges for the potential applications. Indeed, although several research groups reported high quality near lattice matched InAlN/GaN heterostructures[6-10], the growth of InAlN over the full composition range is difficult due to the different physical properties of the binary compounds InN and AlN (bond length, elastic properties, growth temperatures, thermal expansion constants…)[5, 11-13].

Experimentally, the crystallographic degradation of InAlN layers has been reported when the thickness of the layer is increased and some explanations have been reported in the literature[10,14,15]. The first report proposed that the threading dislocations from the GaN could be the main driving force for the alloy degradation through the generation and multiplication of pinholes[10]. Indeed, most of the layers are grown on top of GaN templates which are deposited on sapphire[16.17], silicon[18] or SiC[19] and they contain high densities of crystallographic defects such as threading dislocations[20], inversion domains[21] and stacking faults[22.23]. These defects are transmitted into the growing alloy and may generate typical crystallographic degradations[24]. Other authors have proposed that there could be a critical thickness beyond which the alloy undergoes strain relaxation through crystallographic degradation and generation of extended defects[10]. However, this explanation seems difficult to accept because the reported degradations took place at the indium composition of 17-19%, which is very close to the lattice match on GaN. Moreover, as

reported by Perillat-Marceroz et al.[14] similar degradations occur also in InAlN layers grown on free standing GaN where the influence of the underlying defects cannot be considered as the dominant mechanism due to their low density. The latter authors suggested that the degradation of InAlN layers is a spontaneous phenomenon due to a specific growth mode which systematically leads to the formation of hillocks. It was proposed then that pinholes naturally form and multiply at the coalescence of hillocks[14]. In addition of the crystallographic degradation that has been mainly reported in the Al rich alloy ($In_{0.18}Al_{0.82}N$), phase separation was observed by transmission electron microscopy in indium rich alloys such as $In_{0.72}Al_{0.28}N$[25].

During last years, numerous modelling works have also been devoted to phase diagrams in ternary and quaternary solid solutions[26-30] to determine the instability zone in this alloy; more recently, we demonstrated that biaxial strain influences its miscibility zone[29]. However, structural defects (hillocks and V-defects) were observed independent of the type of strain in InAlN layers for low In compositions of 13.5% (tensile strain), as well as at 19.7% (compressive strain), suggesting that their origin may not be related only to the strain state, but to the intrinsic properties of the InAlN alloy. Therefore, the mechanisms of this degradation are still unclear and need further investigation. Based on first-principles calculations, the formation energies of native defects in AlN and GaN were reported by Mattila and Nieminen[31], Gorczyca et al.[32], Fara et al.[33] and Stampfl and Van de Walle[34.35]. The main conclusion of these investigations was that the self-interstitials and antisites should exhibit high formation energy in wurtzite AlN, whereas the vacancies have the lowest, even for charged defects[36,37,38]. Therefore, it is important to theoretically investigate the possible effects of stable defects in this alloy in order to contribute to a deeper understanding of the mechanism of these degradations.

II. MODELLING PROCEDURE

In this investigation, we have focused on the nitrogen vacancy which is the most stable point defect in the nitride materials[32] and the objective has been to theoretically monitor the behavior of the indium atoms around it. The vacancy is generated by removing a nitrogen atom from the center of a random $In_{0.18}Al_{0.82}N$ alloy in a supercell of 21296 atoms. This size has been previously determined as the low limit of atom number for the minimum dispersion in the energy[29] during our process of relaxation where we use a modified Stillinger Weber type empirical potential, which was previously adapted for the wurtzite nitride compounds[39]. The modification consisted in a parametrization in order to enable efficient atomic simulations of large systems containing wrong, dangling and extra bonds. To this end, the potential was tested through a comparison with ab initio calculations for inversion domain boundaries (IDB), which contained wrongs bonds, as well as a reconstructed IDB and a stacking mismatch boundary (SMB) which could be characterized by four atom rings and dangling bonds, respectively[39]. Using this potential, the calculated elastic properties have also been reported[40].

Prior to the systematic investigation, we have analyzed the behavior of the SW potential in comparison with ab initio procedures as implemented in the VASP commercial software on systems of 127 atoms (with N-vacancy), which are still not so much time expensive. As clearly shown in the supplementary material, the two procedures have a similar trend during the relaxation. Therefore, we can be confident that the results we obtain on large systems using the SW potentials are relevant. In this instance, the large supercells are relaxed until the forces on all atoms become lower than 10^{-15} eV/Å, which makes us choose the final configuration as the most stable. In the relaxed reference supercell containing only the nitrogen vacancy, we then replace the Al atoms around it by In atoms step by step from a radius of 2 to 18 Å, and carry out the SW

relaxation in order to until the most stable configuration is reached. Figure 1 shows the initial configuration of an InN cluster of 14 Å radius generated by substituting all the Al atoms by indium. As all the supercells contain the same number of atoms, the formation energy (ΔE) of the InN cluster is calculated by relating each total energy E_{alloy} (supercell i) to that of the reference, E_{ref} ($\Delta E = E_{alloy} - E_{ref}$).

III. INDIUM CLUSTERING AROUND THE N-VACANCY

A. Energetic behavior

As soon as an indium atom is brought in to substitute an Al one, the energy of the new system decreases. Of course, in order to have the energy reference, we only consider systems with the same atom number. Therefore, one should bear in mind that the indium concentration in the supercell changes with the cluster size. For instance, for a cluster radius of 18 Å, the total number of indium atoms in the cluster is 991, which brings the indium concentration to 27.3%. Then as can be seen in figure 2, the excess energy of the supercell decreases from 2 Å to 6 Å radius up to a ΔE =0.67 eV. For the largest clusters we have considered, the gain in energy is still present but decreases with cluster size. This saddle point of 6 Å radius is interesting; it means that InN clusters of 1.2 Å diameter should have a high probability to form around N vacancies during the growth of InAlN layers.

B. Strain relaxation

In order to try to understand the above energetic behavior, we analyzed the evolution of the atomic bond lengths in the supercell as well as the variation of the lattice parameter inside the cluster.

B.1. Bond lengths

It is interesting to examine the In-N and Al-N bonds in the supercell as a function of the atom position. Considering first the Al-N bond length, we don't have Al inside the cluster; the bond is highly deformed at the interface with the matrix and it attains rapidly the equilibrium length (1.906 Å) in the alloy (fig. 3a). Taking the reference as the Al-N average bond length in the supercell area of $In_{0.18}Al_{0.82}N$, the Al-N bonds are 0.45% compressed for the cluster radius of 14Å. As for the In-N bond length (Fig 3b), in the small cluster sizes (R_c from 2 to 6 Å), it is almost constant, but stretched to reach 2.13 Å inside the cluster slightly more than 2.105 Å in the InAlN alloy. Beyond 6 Å, the compressive strain increases with the cluster size and stabilizes at around 3.5 - 3.6% for the largest considered size. It should be pointed out that the minimum energy at a cluster radius of 6 Å is obtained when the In-N bond length has been established to 2.13 Å (Table I), which is close to the bond length in the indium nitride (2.156 Å).

Around the vacancy, for small clusters, the In-In distance (3.68 Å) is larger than the equilibrium distance in the metallic phase of In (3.25 Å), so there is space for the relaxation of the local strain on In-N bonds. This local strain decreases from 2.07% for R_c=2 Å to 1.31% for R_c= 6 Å. Beyond 6 Å, as can be seen in fig. 3, the In-N bond length is compressed; its length is 2.08 Å for 10 Å and 14 Å. At the same time the distance between In-In atoms starts to increase again (Table I), indicating that the four In atoms just around the N-vacancy enter in the compression state.

B.2. Evolution of the local strain versus the cluster size

To estimate the local strain in the cluster, we calculated the relative change of the lattice parameter a (strain) for different cluster's diameters with respect to the case of the random distribution of In without the N-vacancy, in a cubic cell of $16\ \text{Å} \times 16\ \text{Å} \times 16\ \text{Å}$. The local strain ε as a function of cluster's radius is presented in Fig. 4. As can be seen, the presence of an N-vacancy leads to a local deformation of 0.8%, then when indium atoms are brought in to substitute Al around the vacancy, the strain almost disappears (ε = 0.07%) at the indium nitride cluster radius of 6 Å. For clusters of radius $R_c \leq 6$ Å, the strain is positive, and the area is tensile strained with respect to the InAlN matrix. For $R_c > 6$ Å, the cluster becomes compressed and the deformation goes as high as 4.4% for $R_c = 14$ Å.

IV. EXPERIMENTAL OBSERVATIONS

We have also characterized InAlN layers grown on GaN templates deposited on the (0001) sapphire surface by metalorganic vapour phase epitaxy (MOVPE) by transmission electron microscopy. Whereas tens of samples with various growth conditions have been investigated, in the following, we present the results on two typical InAlN layers, S1 and S2. In S1 sample, the InAlN layer has an indium content of 19% close to the lattice match with GaN and its thickness is 330 nm. For S2, the nominal indium content was 32% and the ternary layer thickness was around 150 nm, corresponding to an expected lattice mismatch of around 1.6%. In an ideal case of strain release by plastic relaxation, this should lead to a periodic network of 60° <11$\bar{2}$0> type dislocations with a theoretical distance of around 200 nm. For transmission electron microscopy (TEM), the cross sections and plan view samples were thinned down to 10μm by mechanical polishing using a Multiprep®, and the electron transparency was obtained by ion milling at 5 kV and mounted on a liquid N2 cold stage. A gradual final step from 3 kV to 100 V was used to decrease ion-beam

damage. Extensive TEM investigation was carried out in the conventional modes in order to identify the crystallographic defects and then through analytical and chemical sensitive high-resolution modes in order to determine the local chemistry and strain state.

The microstructures of the two layers exhibit characteristic features as can be seen in the micrographs of figure 5 which are weak beam images recorded using g = $11\bar{2}0$, in addition to strong strain which corresponds to the white contrast visible inside the InAlN layers. In S1 sample (Fig. 5a), the layer is rough, and the strain predominates towards the surface; from the interface with GaN, the irregular bright parts indicate that the corresponding crystallographic degradation occurs all over the layer without any specific critical thickness and can start even at the interface with the GaN template (arrows). Interestingly, the visible threading dislocations (TD) which have an a component cross the interface as straight lines, meaning that there is not influence of the misfit strain in agreement with the nominal composition of 19% indium.

In S2, the surface roughness is also present as shown in figure 5b, and as can be seen, the structural degradation is initiated starting at the interface with the GaN template. Moreover, in this sample, the contrast of the dislocation lines disappears at the interface, which is clear confirmation that crystalline degradation of the InAlN layer is high from the start. In plane-view, the observations along the $[11\bar{2}3]$ zone axis, where all dislocations should be visible[41]; show only the threading dislocations from the GaN template; they correspond to the visible black line segments (some of them have been underlined by white arrows). In this figure, no single misfit dislocation can be seen inside the InAlN/GaN interface all over this exhibited area of 1.6 μm^2, although, in this layer, the theoretical misfit strain is more than 1.6%. This observation is in contrast to the growth of InGaN on GaN, indeed, at comparable levels of strain, it is has been reported that a network of misfit dislocations forms at the InGaN/GaN interface[42]. This is a clear indication that

the strain relaxation exclusively takes place inside the InAlN alloys, and not at the interface with the underlying GaN template.

Coming back to sample S1, High Angle Annular Dark Field (HAADF) micrographs were recorded along a $<10\bar{1}0>$ zone axis. This method is highly sensitive to variations in the atomic number of constituents in the sample (Z-contrast images). As can be seen in figure 6, numerous areas, which appear to have a spherical shape, exhibit a brighter contrast (In-rich region) than their surroundings indicative of higher average Z composition. Therefore, even inside this nominal $In_{0.19}Al_{0.81}N$ layer, there form indium rich areas in the range of 1-5 nm size (arrows). Inside such areas, the measured In composition can be as high as 35%, whereas only 11% indium is measured inside the dark areas. Columnar features are also visible in this area and the dark ones which are rich in Al, can be seen to originate from these bright clusters. As these columnar features terminate as V defects at the layer surface, it may be concluded that the degradation mechanism of these alloys is related to them and not mainly to the threading dislocations from the GaN template.

V. DISCUSSION AND CONCLUSION

The above observations demonstrate that the strain inside InAlN/GaN heterostructures is not relaxed by the formation of interface defects such as misfit dislocations. The TEM observations show that the strain relaxation takes place randomly inside the alloy without any critical thickness leading to an intrinsic degradation of the crystalline quality of the alloy. Of course, the threading dislocations, as reported earlier[10], participate in this degradation, probably through their interaction with the indium as it has been suggested that In atoms could reduce the energy of c-screw dislocations when they are located at in their core[43]. Moreover, the possible three-dimensional growth mode leading to hillocks[14] build up may not be neglected. The above results highlight the

role of native defects generated during the layer's growth. In particular, the N-vacancy could play a critical role on the In segregation in $In_{0.18}Al_{0.82}N$ towards the formation of In-rich clusters. The calculated excess energy of In-rich cluster in $In_{0.18}Al_{0.82}N$ environment with different size shows that the In-rich cluster is not thermodynamically stable in the perfect structures without defects[44]. However, as seen above, the N-vacancy appears to play a critical role for In aggregation, indeed, the excess energy is increased when In substitute all Al atoms around the vacancy to form InN clusters. When the cluster radius reaches 6 Å, the system has the smallest energy with a decrease of 670 meV. Moreover, this energy stays negative up to largest investigated cluster of 36 Å diameter. Therefore, the aggregation of In atoms around the N-vacancy reduces the energy of the whole system by relaxing the bond length. As for the atomic structure, In-N bonds in the cluster are stretched in comparison with the bulk alloy due to the effect of N-vacancy.

From the TEM observations, 1 to 5 nm indium rich clusters are present from the beginning of the InAlN alloy growth. Of course, these clusters participate in the modification of the local chemical uniformity as seen in the Z contrast image. Their connection to columnar features is obvious evidence that they are at the origin of the subsequent degradation of the grown film.

Are these clusters related to N vacancies? The TEM investigation cannot attest this, but the the above calculations show that this is highly probable. Therefore, considering our observations and associated modelling, it may be suggested that the growth of the InAlN layer proceeds with more and more indium atoms gathering around the N-vacancy, thus depleting the surroundings and leading to possible formation of Al rich columns, associated chimneys, as well as final degraded hillocks and surface pinholes. The next steps will be to take into account larger systems in our simulations and to investigate the kinetics of this intrinsic degradation of the InAlN layers using molecular dynamics procedures. Indeed, at this point, we need to investigate at which stage

the degradation takes place, does it start during the growth itself, the cooling: this is still an open question which needs to be addressed in the next steps. The only point we are sure of, is that after cooling, the structure and composition of the final layers is completely set and highly stable.

SUPPLEMENTARY MATERIAL

In this part, we demonstrate the similar behavior of the SW potential in comparison with ab initio energetics when Al atoms are replaced by indium atoms to simulate the initial formation of an indium rich cluster. To this end, 128 atoms supercell are handled within the ab-initio procedures, the similar trend permits us to carry out the modelling on much larger supercells using the SW empirical potential.

■ AUTHOR INFORMATION

Corresponding Author

* E-mail: ranim.mohamad@ensicaen.fr

■ ACKNOWLEDGMENTS

This work has been partly supported by the EU under project OSIRIS contract ECSEL-JU, GA: 662322. The calculations were carried out in the « Centre Régional Informatique et d'Applications Numériques de Normandie » "CRIANN" (www.criann.fr) under project number: 2016009.

■ REFERENCES

[1] S. Nakamura, M. Senoh, N. Iwasa and S. Nagahama, Jpn. J. Appl. Phys. **34**, L797 (1995).

[2] S. Nakamura, M. Senoh, S.-I. Nagahama, N. Iwasa, T. Yamada, T. Matsushita and H. Kiyoku, Jpn. J. Appl. Phys. **35**, L74 (1996).

[3] M. A. Khan, S. Shur and Q. Chen, Appl. Phys. Lett. **68**, 3022 (1996).

[4] A. Fridman, A. Chirokov and A. Gutsol, J. Phys. D: Appl. Phys. **38**, R1 (2005).

[5] I. Vurgaftman and J. R. Meyer, J. Appl. Phys. **94**, 3675 (2003).

[6] J. F. Carlin, C. Zellweger, J. Dorsaz, S. Nicolay, G. Christmann, E. Feltin, R. Butté and N. Grandjean, Phys. Stat. Sol. (b). **242**, 2326 (2005).

[7] A. Dadgar, F. Schulze, J. Blasing, A. Diez, A. Krost, M. Neuburguer, E. Kohn, I. Daumiller and M. Kunze, Appl. Phys. Lett. **85**, 5400 (2004).

[8] K. Bejtka, R. W. Martin, I. M. Watson, S. Ndiaye and M. Leroux, Appl. Phys. Lett. **89**, 191912 (2006).

[9] I. M. Watson, C. Liu, E. Gu, M. D. Dawson, P. R. Edwards and R. W. Martin, Appl. Phys. Lett. **87**, 151901 (2005).

[10] Z. T. Chen, K. Fujita, J. Ichikawa and T. Egawa, J. Appl. Phys. **111**, 053535 (2012).

[11] G. A. Slack, R. A Tanzilli, R. O. Pohl and J. W. Vandersande, J. Phys. Chem. Solids **48**, 641 (1987).

[12] E. K. Sichel and J. I. Pankove, J. Phys. Chem. Solids **38**, 330 (1977).

[13] S. Krukowski, A. Witek, J. Adamczyk, J. Jun, M. Bockowski, I. Grzegory, B. Lucznik, G. Nowak, M. Wroblrwski, A. Presz, S. Gierlotka, S. Stelmach, B. Palosz, S. Porowski and P. Zinn, J. Phys. Chem. Solids **289** (1998).

[14] G. Perillat-merceroz, G. Cosendey, J. Carlin, R. Butté and N. Grandjean, J. Appl. Phys. **113**, 063506 (2013).

[15] Q. Y. Wei, T. Li, Y. Huang, Z. T. Chen, T. Egawa and F. A. Ponce, Appl. Phys. Lett. **100**, 092101 (2012).

[16] R. Goldhahn, P. Schley, A. T. Winzer, G. Gobsch, V. Cimalla, O. Ambacher, M. Rakel, C. Cobet, N. Esser, H. Lua and W. J. Schaff, Phys. Stat. Sol. (a) **203**, 42 (2006).

[17] P. Ruterana, Y. Potin, B. Barbaray and G. Nouet, Philos. Mag. A **80**, 937 (2000).

[18] C. Hums, A. Gadanecz, A. Dadgar, J. Bläsing, H. Witte, T. Hempel, A. Dietz, P. Lorenz, S. Krischok, J. A. Schaefer, J. Christen and A. Krost, Mater. Res. Soc. Symp. Proc. **1068**, C04-03 (2008).

[19] P. Vermaut, P. Ruterana, G. Nouet and H. Morkoç, Inst. Phys. Conf. Ser. **146**, 289 (1995).

[20] V. Potin, P. Ruterana, G. Nouet, R. Pond and H. Morkoc, Phys. Rev. B **61**, 5587 (2000).

[21] V. Potin, G. Nouet and P. Ruterana, Appl. Phys. Lett. **74**, 947 (1999).

[22] V. Potin, P. Ruterana and G. Nouet, Mat. Sci. and Eng. B **82**, 114 (2001).

[23] P. Ruterana, B. Barbaray, A. Béré, P. Vermaut, A. Hairie, E. Paumier, G. Nouet, A. Salvador, A. Botchkarev and H. Morkoç, Phys. Rev. B **59**, 24 (1999).

[24] H. Ben Ammar, A. Minj, M.- P Chauvat, P. Gamarra, C. Lacam, M. Morales and P. Ruterana, J. Microsc. **268**, 269 (2017).

[25] J. Palisaitis, C. Hsiao, L. Hultman, J. Birch and P. O. Å. Persson, Sci. Rpe. 7 **4439** (2017).

[26] G. B. Stringfellow, J. Cryst. Growth **27**, 21 (1974).

[27] K. Osamura, N. Shigehisa and Y. Murakami, J. Appl. Phys. **46**, 3432 (1975).

[28]T. Matsuoka, J. of Crystal Growth **190**, 19 (1998).

[29] R. Mohamad, A. Béré, J. Chen and P. Ruterana, Phys. Stat. Sol. (a) **214**, 1600752 (2017).

[30] R. Mohamad, A. Béré, V. Hounkpati, P. Gamarra, J. Chen and P. Ruterana, Phys. Stat. Sol. (b) **255**, 1700394 (2018).

[31] T. Mattila and R. M. Nieminen, Phys. Rev. B **55**, 9571 (1997).

[32] I. Gorczyca, A. Svane and N. E. Christensen, Phys. Rev. B **60**, 8147 (1999).

[33] A. Fara, F. Bernardini and V. Fiorentini, J. Appl. Phys. **85**, 2001 (1999).

[34] C. Stampfl and C. G. Van de Walle, Phys. Rev. B **65**, 155212 (2002).

[35] C. Stampfl and C. G. Van de Walle, Appl. Phys. Lett. **72**, 459 (1998).

[36] S. Limpijumnong and C. G. Van de Walle, Phys. Rev. B, **69**, 035207 (2004).

[37] K. Laaksonen, M. G. Ganchenkova and R. M. Nieminen, J. Phys.: Condens. Matter **21**, 15803 (2009).

[38] J. Kioseoglou, V. Pontikis, Ph. Komninou, Th. Pavloudis, J. Chen and Th. Karakostas, J. Phys.: Condens. Matter, **27** 125006 (2015).

[39] N. Aïchoune, V. Potin, P. Ruterana, A. Hairie, G. Nouet and E. Paumier, Comput. Mater. Sci. **17**, 380 (2000).

[40] H. Lei, Ph.D. thesis, University of Caen, France 2009

[41] K. Pantzas, G. Patriarche, G. Orsal, S. Gautier, T. Moudakir, M. Abid, V. Gorge, Z. Djebbour, P. L. Voss and A. Ougazzaden, Phys. Stat. Sol. (a) **209**, 25 (2012).

[42] R. Liu, J. Mei, S. Srinivasan, H. Omiya, F. A. Ponce, D. Cherns, Y. Narukawa and T. Mukai, Jpn. J. Appl. Phys. **45**, L549 (2006).

[43] H. Lei, J. Chen and P. Ruterana, Appl. Phys. Lett. **96**, 161901 (2010).

[44] R. Mohamad, Ph.D. thesis, University of Caen, France 2018.

Figures captions:

Figure 1. The R=14Å supercell with an InN cluster embedded in an $In_{0.18}Al_{0.82}N$ random matrix.

Figure 2. Cluster radius dependence of excess energy of In-rich cluster and N-vacancy in the environment of $In_{0.18}Al_{0.82}N$ for the supercell of 21295 atoms.

Figure 3. Profile of Al-N and In-N bond lengths as a function of distance from the cluster's center with radius 2 Å (black), 4 Å (red), 6 Å (green), 10 Å (blue), 14 Å (cyan) and 18 Å (purple).

Figure 4. The local strain on lattice constant a as a function of cluster radius

Figure 5. Micrographs of the two heterostructures, the cross section images were recorded with g= 11-20: a) S1 exhibits a rough surface with strained layer which has an irregular limit towards the interface; b) S2, the layer is rough, the degradation starts at the AlInN/GaN interface; c) S2: Plan-view micrograph along the $[11\bar{2}3]$ zone axis, threading dislocations are visible as black line segments (arrows).

Figure 6. HAADF micrograph recorded along a $<10\bar{1}0>$ zone axis close to the interface AlInN/GaN in sample S1, bright contrast corresponds to indium rich areas (see arrows).

Table:

Table I: The deformation in (%) on In-N bonds around N-vacancy with respect to the equilibrium state 2.156 Å and In-In distance, as function of cluster radius.

R_c (Å)	In-N deformation (%)	In-In distance (Å)
2	2.07	-
4	1.98	3.68
6	1.31	3.25
7	2.55	3.34
8	3.25	3.41
10	3.52	3.52
14	3.53	3.53

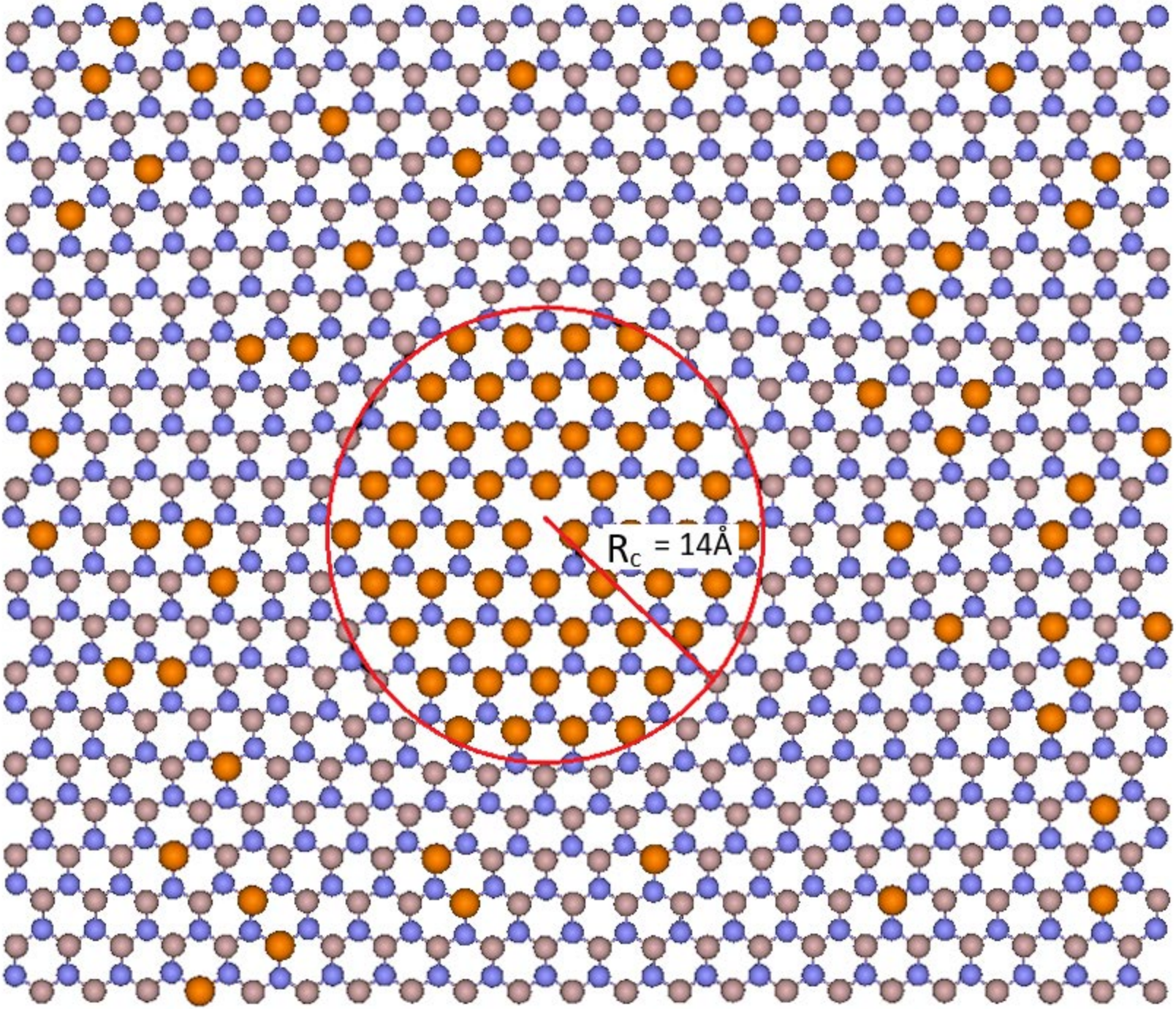
R_c = 14Å

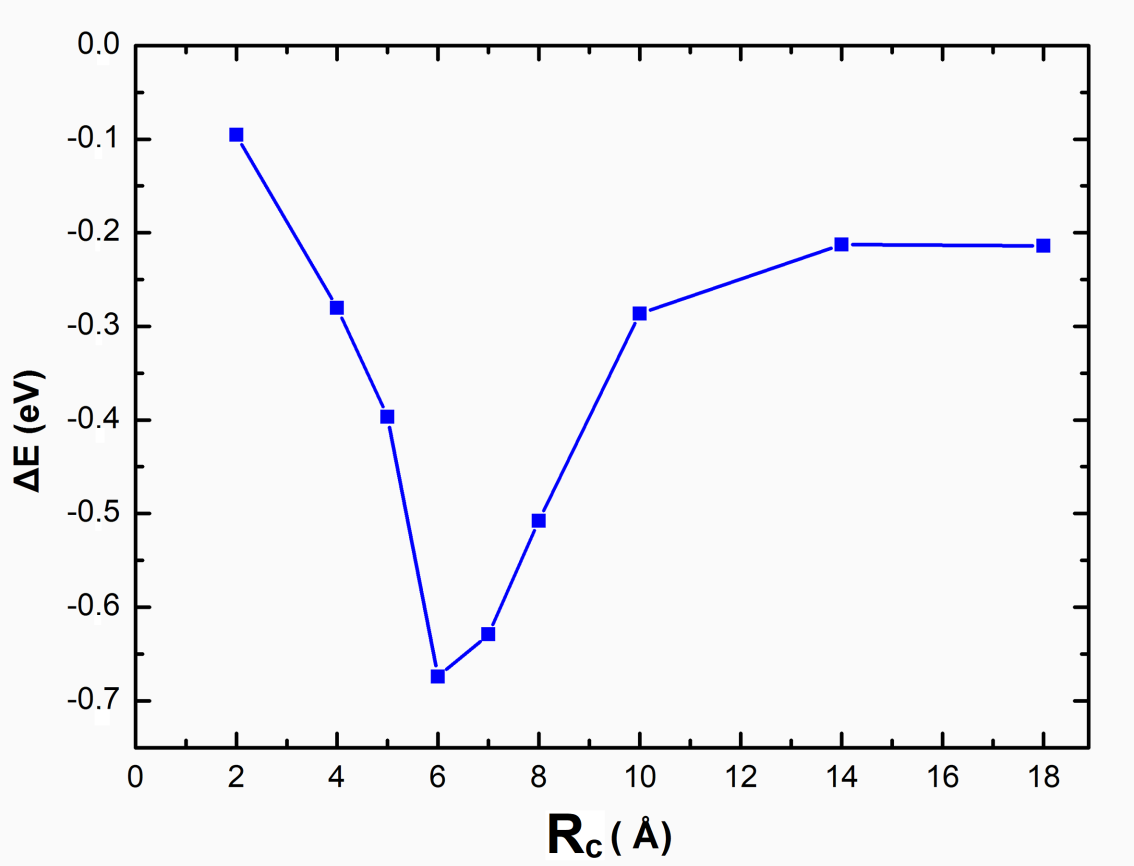
0.0
-0.1
-0.2
-0.3
-0.4
-0.5
-0.6
-0.7
ΔE (eV)
0
2
4
6
8
10
12
14
16
18
Rc (Å)

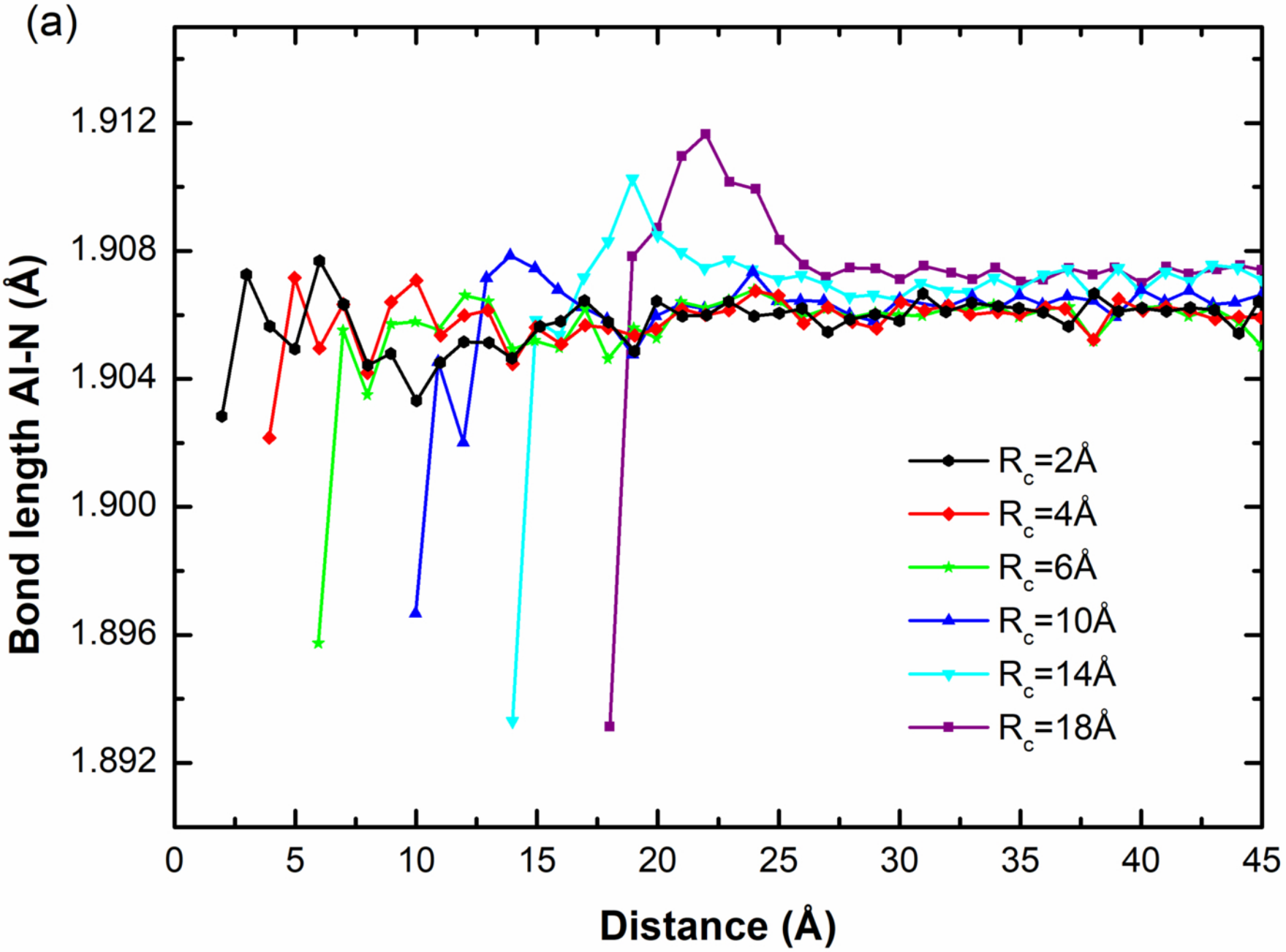
(a)
Bond length Al-N (Å)
1.912
1.908
1.904
1.900
1.896
1.892
0
5
10
15
20
25
30
35
40
45
Distance (Å)
R_c=2Å
R_c=4Å
R_c=6Å
R_c=10Å
R_c=14Å
R_c=18Å

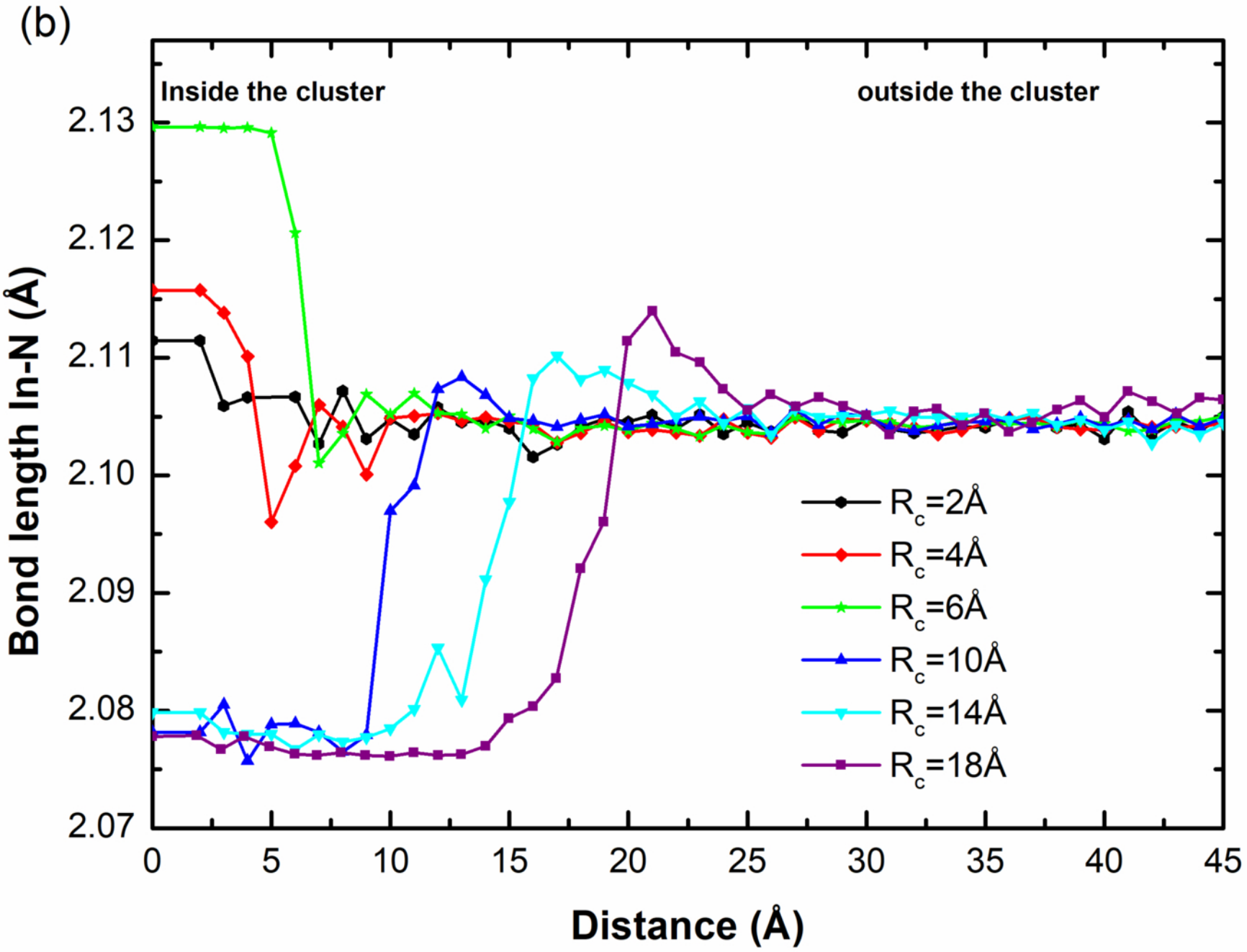
(b)
Inside the cluster
outside the cluster
Bond length In-N (Å)
2.13
2.12
2.11
2.10
2.09
2.08
2.07
0
5
10
15
20
25
30
35
40
45
Distance (Å)
R_c=2Å
R_c=4Å
R_c=6Å
R_c=10Å
R_c=14Å
R_c=18Å

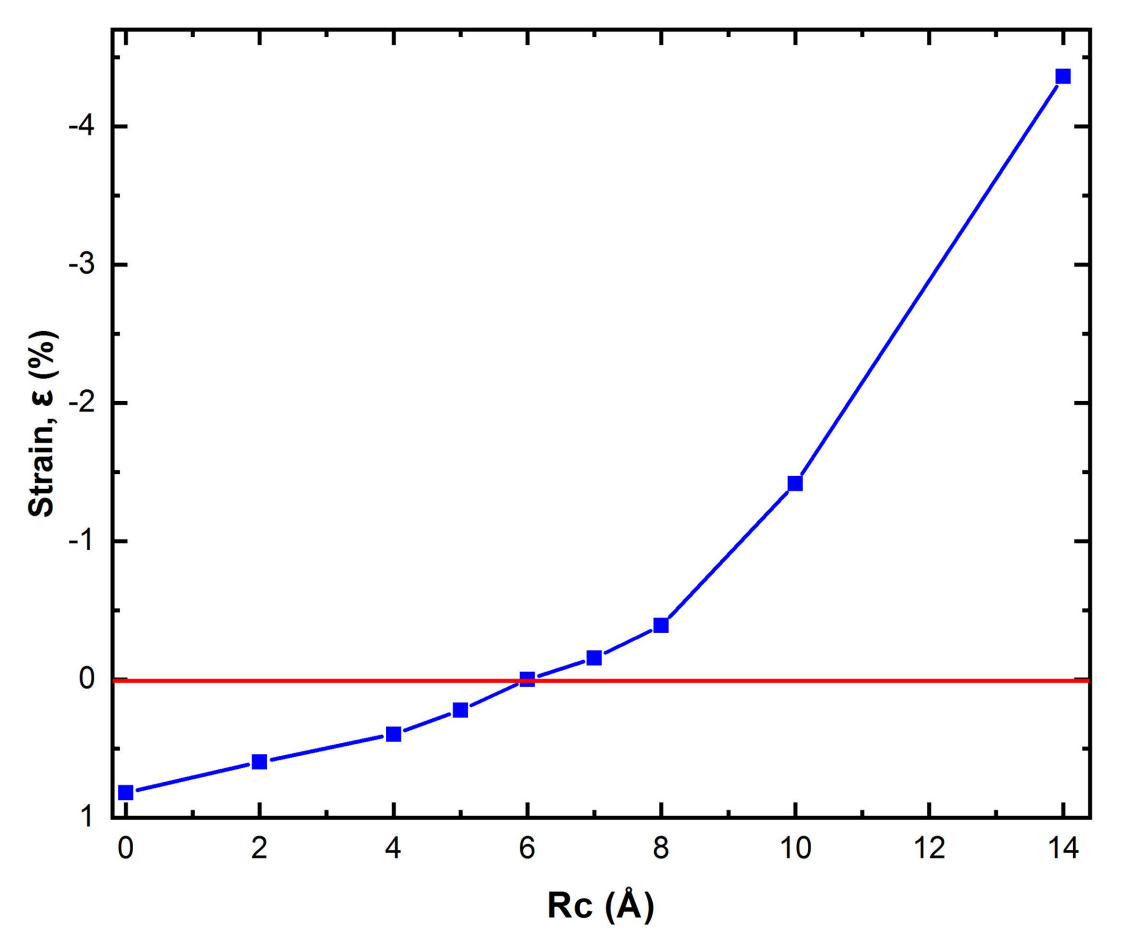
-4
-3
-2
-1
0
1
Strain, ε (%)
0
2
4
6
8
10
12
14
Rc (Å)

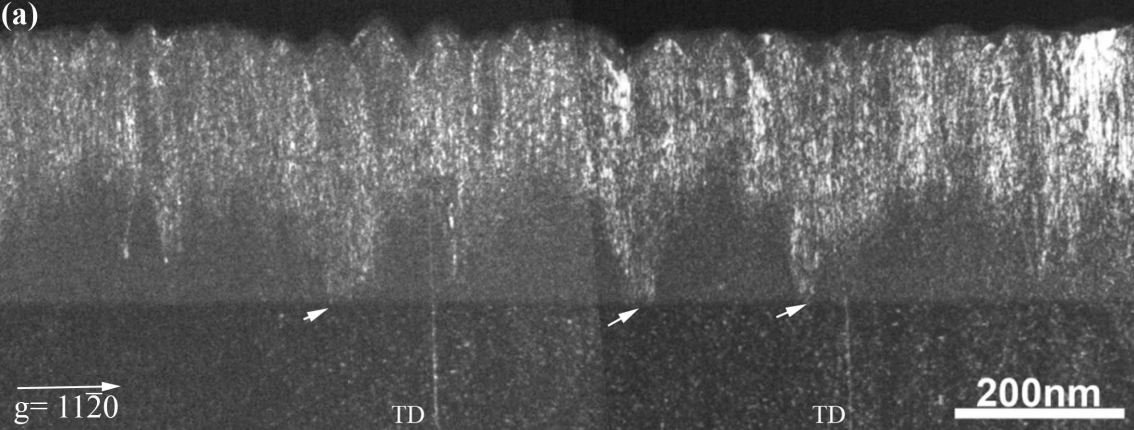
(a)
g= 1120
TD
TD
200nm

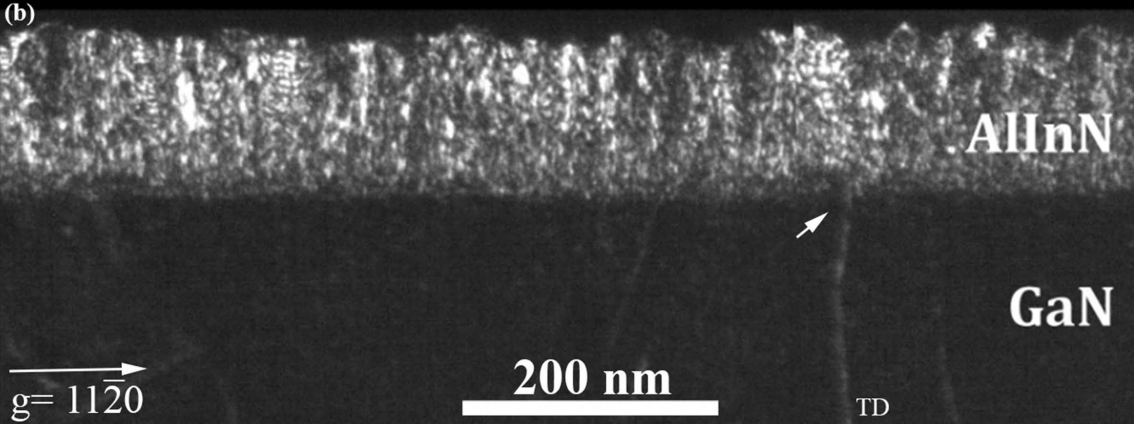
(b)
AlInN
GaN
200 nm
g= 11$\bar{2}$0
TD

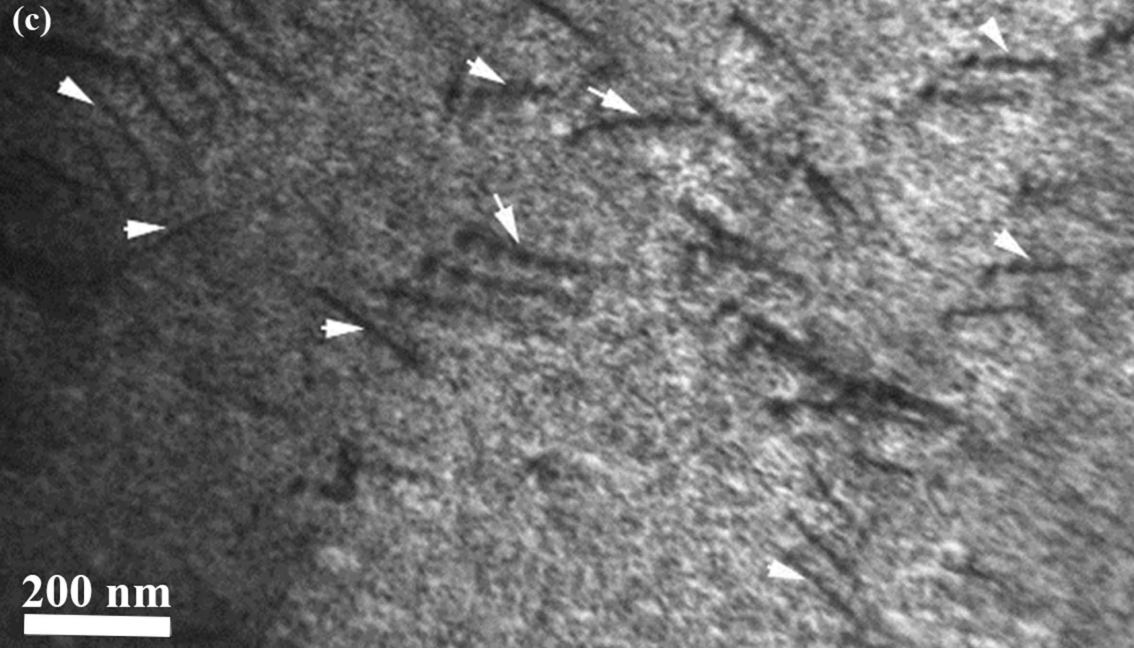
(c)
200 nm

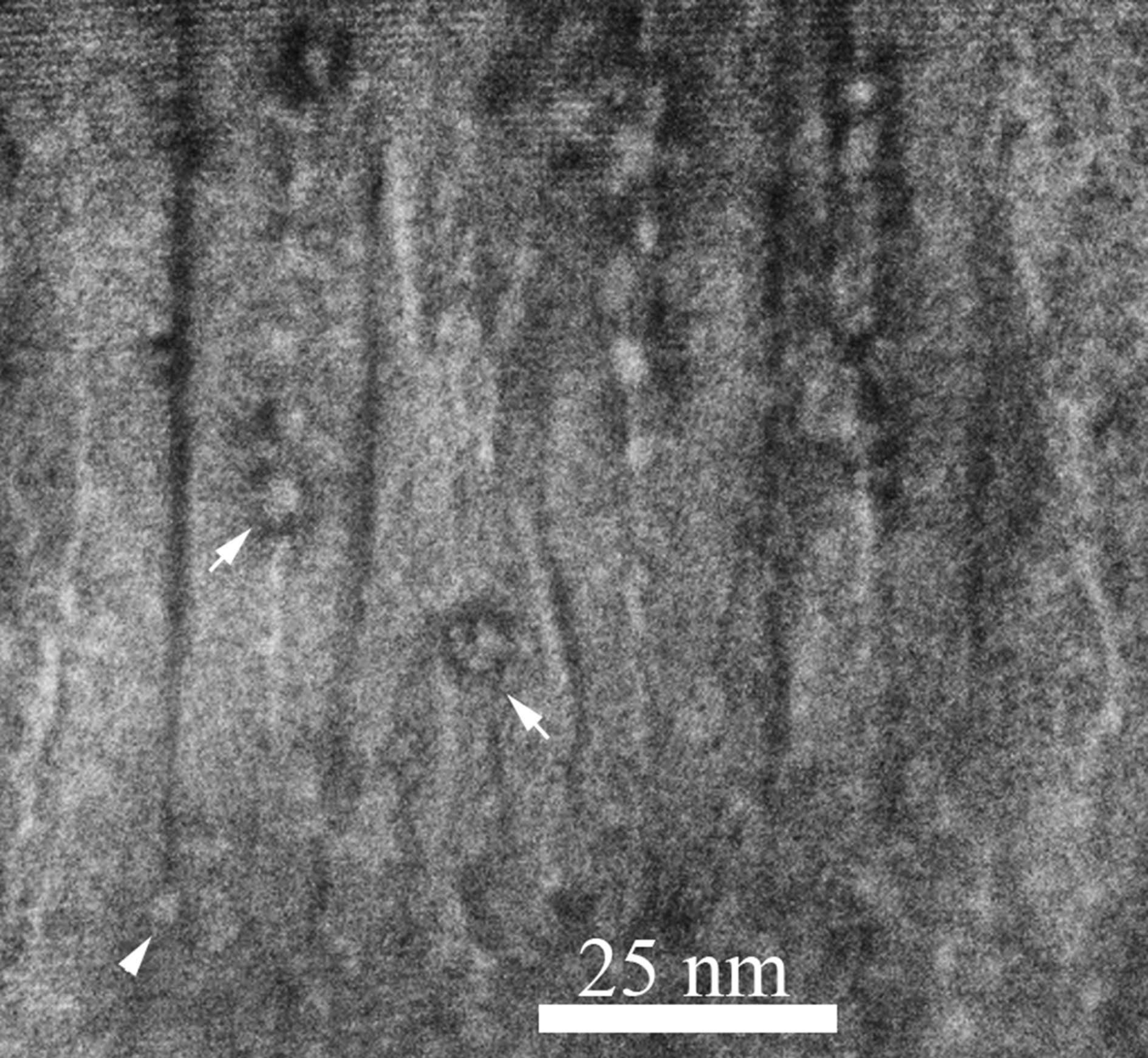
25 nm